Neuron, Vol. 48, 757–771, December 8, 2005, Copyright ©2005 by Elsevier Inc. DOI 10.1016/j.neuron.2005.11.005

Polarized Secretory Trafficking Directs Cargo for Asymmetric Dendrite Growth and Morphogenesis

April C. Horton,[2] Bence Rácz,[4] Eric E. Monson,[3] Anna L. Lin,[3] Richard J. Weinberg,[4,5] and Michael D. Ehlers[1,2,*]
[1] Howard Hughes Medical Institute
[2] Department of Neurobiology
[3] Department of Physics
Duke University Medical Center
Durham, North Carolina 27710
[4] Department of Cell & Developmental Biology and
[5] Department of Neuroscience Center
University of North Carolina
Chapel Hill, North Carolina 27599

Summary

Proper growth of dendrites is critical to the formation of neuronal circuits, but the cellular machinery that directs the addition of membrane components to generate dendritic architecture remains obscure. Here, we demonstrate that post-Golgi membrane trafficking is polarized toward longer dendrites of hippocampal pyramidal neurons in vitro and toward apical dendrites in vivo. Small Golgi outposts partition selectively into longer dendrites and are excluded from axons. In dendrites, Golgi outposts concentrate at branchpoints where they engage in post-Golgi trafficking. Within the cell body, the Golgi apparatus orients toward the longest dendrite, and this Golgi polarity precedes asymmetric dendrite growth. Manipulations that selectively block post-Golgi trafficking halt dendrite growth in developing neurons and cause a shrinkage of dendrites in mature pyramidal neurons. Further, disruption of Golgi polarity produces neurons with symmetric dendritic arbors lacking a single longest principal dendrite. These results define a novel polarized organization of neuronal secretory trafficking and demonstrate a mechanistic link between directed membrane trafficking and asymmetric dendrite growth.

Introduction

Proper dendritic development is a prerequisite for appropriate formation of neural circuits (Jan and Jan, 2003). Many of the genetic (Grueber et al., 2003), signal-dependent (Whitford et al., 2002), and cytoskeletal bases (Van Aelst and Cline, 2004) for dendritic outgrowth have been elucidated. An overlooked aspect of neuronal development is the addition of plasma membrane required to construct a complex surface area 10,000 times greater than typical animal cells, extending highly branched structures hundreds of microns from the cell body (Horton and Ehlers, 2004). The major sites of synthesis of lipid and protein components of the plasma membrane are the organelles of the secretory pathway, including the endoplasmic reticulum (ER) and Golgi apparatus. How membrane trafficking through the secretory pathway is organized to support the formation and maintenance of complex asymmetric dendritic arbors remains obscure.

A requirement for membrane trafficking in the formation of neuronal processes was initially indicated for the growth of axons (Jareb and Banker, 1997). However, dendrites and axons are remarkable for their different morphological and functional properties, and an increasing body of work indicates that axonal and dendritic outgrowth are regulated by distinct mechanisms (Polleux et al., 2000). Indeed, the axon and dendrites on a single neuron may have opposing responses to secreted guidance molecules such as semaphorin 3A, an effect that requires the polarized distribution of downstream signaling molecules (Polleux et al., 2000). Further, during development, neurons may switch irreversibly from an axonal to a dendritic growth mode (Goldberg et al., 2002), implying two distinct modes of outgrowth. Finally, although neurons typically have only a single axon, they usually have multiple dendrites that may be morphologically and functionally distinct from one another. For example, pyramidal neurons of the cerebral cortex and hippocampus have a single apical dendrite that extends hundreds of microns toward the pia and several smaller, shorter basolateral dendrites that receive distinct synaptic inputs (Whitford et al., 2002). The signaling cascades and trafficking pathways that specify axons versus dendrites are becoming clarified (de Anda et al., 2005; Nishimura et al., 2004; Schwamborn and Puschel, 2004; Shi et al., 2003), but little is known of the cellular events that generate distinct dendrites with differing sizes and geometries.

In other cell types, directed secretory trafficking regulates the growth of plasma membrane domains involved in processes as diverse as yeast cell budding, immune cell function, and cell migration (Bergmann et al., 1983; Etienne-Manneville and Hall, 2003; Kupfer et al., 1983). Recent studies have shown that the secretory pathway in neurons has a spatial distribution unique among mammalian cells (Gardiol et al., 1999; Horton and Ehlers, 2003; Pierce et al., 2001). Rather than being a single-copy perinuclear organelle as in most cell types, the neuronal Golgi apparatus is instead composed of both Golgi stacks in the cell body and discrete Golgi "outposts" in dendrites. These dendritic Golgi outposts may be synapse-associated (Gardiol et al., 1999; Pierce et al., 2001), and their appearance in dendrites is developmentally regulated, with dendritic Golgi becoming evident during periods of rapid dendritic outgrowth and synapse formation (Horton and Ehlers, 2003). Notably, the number of dendritic ER exit sites, where secretory cargo buds from the ER en route to the Golgi, also increases during dendritic outgrowth (Aridor et al., 2004), and TGN organelles in dendrites localize at sites of neuron-neuron contact (Sytnyk et al., 2002). These observations point to the possibility that the spatial distribution of dendritic secretory elements may contribute to dendrite morphogenesis.

Here, we investigate the spatial and temporal organization of secretory trafficking in dendrites and its role in

*Correspondence: ehlers@neuro.duke.edu

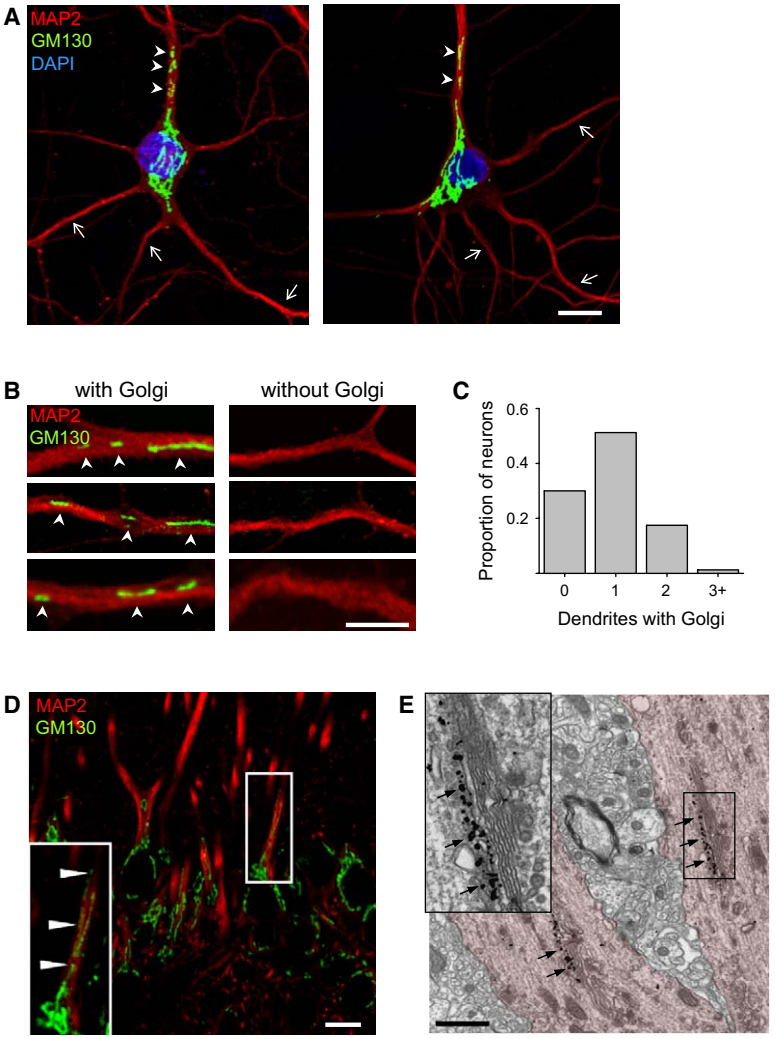

Figure 1. Golgi Outposts Concentrate in One Dendrite

(A) Cultured hippocampal neurons (10 DIV) immunostained for the *cis*-Golgi protein GM130 (green), the dendritic marker MAP2 (red), and DAPI (blue). GM130 labeling is present in a single dendrite (arrowheads) and is excluded from other dendrites on the same neuron (arrows). Scale bar, 10 μm.

(B) Pairs of dendrites from three different neurons show the presence of GM130 (green) in one dendrite (left), whereas GM130 is absent from other dendrites on the same neuron (right). Scale bar, 10 μm.

(C) Quantification of a set of 80 cultured hippocampal neurons (10 DIV), stained as in (A) and (B) and classified into groups based on the number of dendrites containing GM130-positive Golgi outposts.

(D) Adult rat hippocampus stained for MAP2 (red) and GM130 (green). Arrowheads (inset) indicate GM130 labeling in apical dendrites of CA1 pyramidal neurons. Scale bar, 10 μm; inset, 5.5 μm.

(E) Immunogold labeling for GM130 in adult rat hippocampus shows GM130-labeled Golgi outposts in the apical dendrite of a CA1 pyramidal neuron in vivo. Outposts are composed of stacks of cisternae with gold particles decorating the cis-face (arrows) as expected. Scale bar, 1 μm; inset, 500 nm.

dendrite growth and morphogenesis. Using a combination of live-cell imaging, electron microscopy, and quantitative morphometric analysis in cell culture, brain slices, and rodent brain, we demonstrate that post-Golgi secretory trafficking in neurons is polarized toward longer, more complex dendrites and is required for dendritic outgrowth. In hippocampal neurons, Golgi outposts localize selectively to dendritic branchpoints and are typically present in only one long dendrite, which in vivo is the apical dendrite. Within the cell body, the Golgi apparatus orients toward the longest dendrite, and post-Golgi secretory cargo is delivered predominantly toward this principal dendrite. This Golgi polarization precedes and is required for the formation of polarized dendritic arbors. Surprisingly, somatic Golgi has no polarity toward the axon; Golgi outposts are excluded from axons, and axonal outgrowth proceeds despite secretory pathway manipulations that prevent dendritic outgrowth, demonstrating specificity for anterograde secretory trafficking in the construction of dendritic, and not axonal, arbors. These results demonstrate an unanticipated spatial organization of neuronal secretory trafficking and identify polarized trafficking as a novel mechanism for asymmetric dendritic growth and morphogenesis.

Results

Dendritic Golgi Partitions to Longer Dendrites

Discrete Golgi elements capable of transporting secretory cargo are present in dendrites (Horton and Ehlers, 2003). To determine whether all dendrites or only a subset contain such Golgi outposts, we stained 10 day in vitro (DIV) hippocampal neurons for the dendritic marker MAP2 and for GM130, a marker of the *cis*-Golgi compartment (Figure 1A). Although the population of neurons examined had on average 5 ± 1.7 dendrites (n = 80), only one or two dendrites had detectable dendritic Golgi (Figure 1A, arrowheads). This selective localization of Golgi elements to single dendrites was readily observed in distal dendrites examined from individual neurons (Figure 1B). Quantitative analysis revealed that 70% of DIV 10 hippocampal neurons had dendritic Golgi. Of these, most had Golgi in only a single dendrite, with nearly all the remainder having Golgi elements in two dendrites (Figure 1C). Grouped together, 51% of DIV 10 hippocampal neurons had Golgi in a single dendrite, 19.5% had Golgi in two dendrites, and 29.5% had no dendritic Golgi (Figure 1C). The exclusion of Golgi from some dendrites was not due to the diameter of the proximal dendrite because dendrites of similar width on the

same neurons could either contain (Figure 1B, left) or lack (Figure 1B, right) dendritic Golgi. Counting all dendrites together, only 17.7% possessed detectable Golgi outposts. This segregation of Golgi to particular dendrites is in sharp contrast to the distribution of other membrane bound organelles, including endoplasmic reticulum and ER exit sites (Aridor et al., 2004; Horton and Ehlers, 2003), as well as endosomes and mitochondria (Figure S1), which are present in all dendrites. Golgi outposts were also detectable in apical dendrites of CA1 pyramidal neurons in adult rat hippocampus dual labeled for MAP2 and GM130 (Figure 1D). To examine the ultrastructure of dendritic Golgi in the adult brain, we performed immunogold electron microscopy on rat hippocampus. Discrete Golgi stacks labeled for GM130 were readily discernable in the proximal portions of pyramidal neuron apical dendrites, extending as far as 100 μm from the soma (Figure 1E), but were seldom observed in basolateral dendrites (data not shown). Thus, Golgi is present in only a small fraction of neuronal dendrites—typically only one per neuron. In pyramidal neurons in vivo, this is the apical dendrite.

The Golgi provides a potential source of membrane components for localized cell growth (Prigozhina and Waterman-Storer, 2004). To determine whether the presence of Golgi outposts predicts dendrite shape, we performed morphometric analysis of dendritic length and complexity. Inspection of individual neurons revealed that dendrites containing Golgi elements were longer and more complex than dendrites lacking Golgi (Figure 2A). Direct measurement revealed that Golgi was present in the longest dendrite on 86% of neurons. Further quantitative analysis showed that the presence of Golgi corresponded to a 3-fold increase in dendritic length (277 ± 16 μm versus 90 ± 4 μm, $p < 0.001$) (Figure 2B). Moreover, dendrites containing Golgi were more than twice as long as their longest counterpart lacking Golgi on the same cell (306 ± 6 μm versus 148 ± 10 μm, $p < 0.001$) (Figure 2C).

Another morphological characteristic of mature neurons is the development of a highly branched dendritic arbor. To determine whether the spatial organization of neuronal Golgi was related to dendritic complexity, we counted the number of dendritic tips, finding that dendrites containing Golgi were more complex than dendrites lacking Golgi (6.0 ± 0.4 versus 2.4 ± 0.1 tips per dendrite, $p < 0.001$) (Figure 2D). Further, comparing the most complex dendrite with Golgi to the most complex dendrite without Golgi on the same neuron revealed an increase in complexity in those dendrites containing Golgi outposts (6.6 ± 0.4 versus 3.9 ± 0.3, $p < 0.001$) (Figure 2E). Together, these data show that the asymmetry of Golgi distribution corresponds to asymmetric patterns of dendritic outgrowth, with dendritic Golgi present in the longer, more complex dendrites.

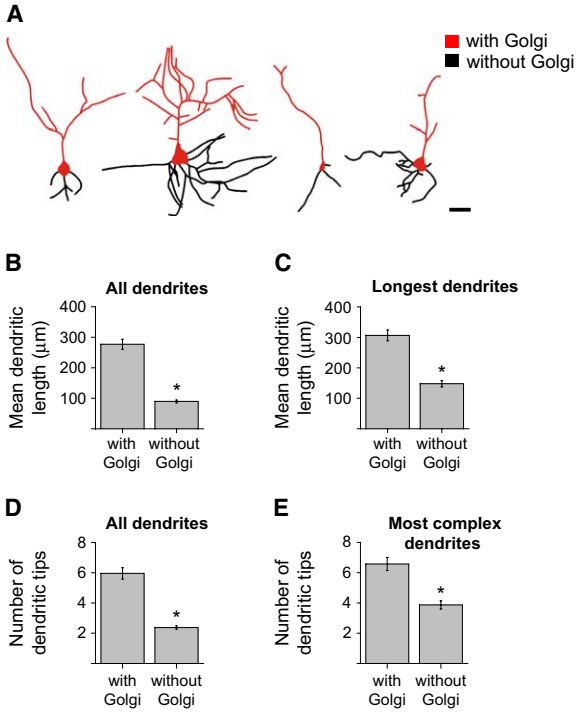

Figure 2. Dendrites with Golgi Outposts Are Longer and More Complex

(A) Camera lucida drawings of dendrites from 10 DIV hippocampal neurons. Dendrites were defined as MAP2-positive processes and classified according to the presence or absence of GM130-labeled dendritic Golgi outposts. The entire length of each dendrite was then color coded to indicate the presence (red) or absence (black) of Golgi. Scale bar, 20 μm.

(B) Mean lengths of all dendrites with and without Golgi. n = 407 dendrites on 80 neurons; asterisk, $p < 0.001$. Data represent means ± SEM.

(C) Mean lengths of the longest dendrite with Golgi and the longest dendrite without Golgi on each neuron. n = 112 dendrites on 56 neurons; asterisk, $p < 0.001$. Data represent means ± SEM.

(D) Mean number of dendritic tips of all dendrites with and without Golgi. Fewer dendritic tips indicates less branching. n = 407 dendrites on 80 neurons; asterisk, $p < 0.001$. Data represent means ± SEM.

(E) Mean number of dendritic tips on the most complex dendrite with Golgi and the most complex dendrite without Golgi on each neuron. n = 112 dendrites on 56 neurons; asterisk, $p < 0.001$. Data represent means ± SEM.

Golgi in the Soma Orients toward Longer Dendrites

Although dendritic Golgi outposts are a conspicuous feature of pyramidal neurons (Figure 1C), somatic Golgi in the cell body makes up the majority of the total Golgi apparatus (Figure 1) (Horton and Ehlers, 2003). To test whether the somatic Golgi polarizes toward longer dendrites, we analyzed the radial distribution of GM130-labeled *cis*-Golgi in the cell body (Figure S2). For this analysis, a line drawn between the center of mass of the neuronal soma and the emergence point of the longest dendrite was defined as $\theta = 0°$ (Figure 3A). The distribution of Golgi relative to the axis of the longest dendrite was then averaged across a population of neurons. This analysis revealed that in DIV 10 hippocampal neurons, the somatic Golgi was polarized toward the longest dendrite (Figure 3B). The probability of Golgi being located in the quadrant of the neuronal soma immediately adjacent to the emergence point of the longest dendrite was twice that of other regions of the cell body (Figure 3B, inset).

To test whether this polarized organization of Golgi in the soma occurs in vivo, we examined the distribution of GM130-labeled *cis*-Golgi in pyramidal neurons in adult rat somatosensory cortex. In cortex and hippocampus, the longest dendrite of pyramidal neurons is the apical

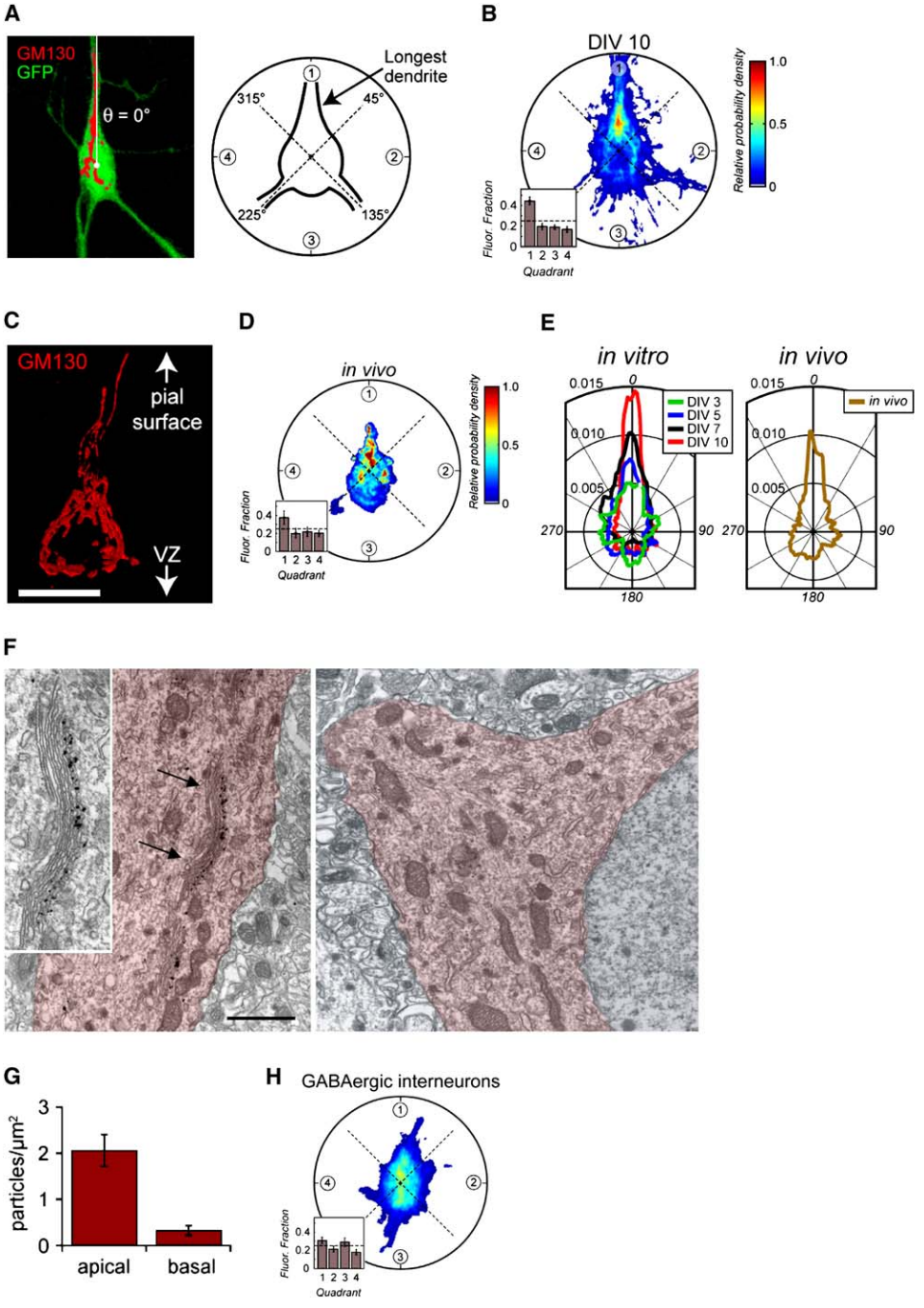

Figure 3. Somatic Golgi Is Polarized Toward the Longest Dendrite In Vitro and the Apical Dendrite In Vivo.

(A) (Left) Hippocampal neuron (10 DIV) expressing EGFP (green) and stained for GM130 (red). The longest dendrite defines θ = 0°. Note the extension of the Golgi into this dendrite. Scale bar, 10 μm. (Right) To produce a radial coordinate system, we defined the center of the neuronal soma as the origin, and the base of the longest dendrite was defined as θ = 0°. The somatic region was divided into four quadrants (circled numbers) as shown. See Experimental Procedures and Figure S2 for details.

(B) Summation of images corresponding to GM130-labeled Golgi from hippocampal neurons (10 DIV, n = 32) aligned as in (A). Pseudocolor scale for summed fluorescence intensity is shown at right. Note that Golgi fluorescence intensity is polarized toward the longest dendrite (θ = 0°) in quadrant one. The inset bar graph shows the fraction of fluorescence present in each quadrant.

(C) GM130 (red) staining in a layer V pyramidal neuron in a section from adult rat somatosensory cortex. The image is oriented with respect to the pial surface and ventricular zone (VZ), as indicated by the arrows. Scale bar, 10 μm.

(D) Summation of GM130 images from layer V pyramidal neurons in adult mouse cortex stained in tissue section (n = 13). Neurons expressing GFP were aligned as described above, except that the apical dendrite was defined as θ = 0°. Note the enhanced density of GM130-labeld Golgi in the quadrant of the soma immediately adjacent to the apical dendrite.

(E) Cumulative angular probability distributions of Golgi fluorescence with respect to the longest dendrite in primary neuron cultures (left) or the apical dendrite in brain sections (right). Angles are defined as in (A).

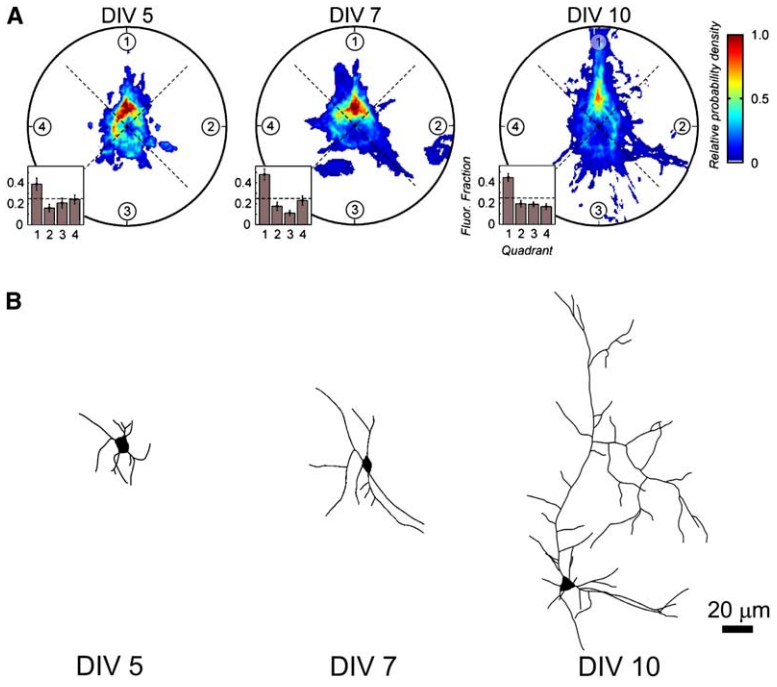

Figure 4. Golgi Polarity Precedes Dendrite Polarity

(A) Development of Golgi polarity in the cell body. Summation of GM130-labeled Golgi images in DIV 5 (n = 25), DIV 7 (n = 25), and DIV 10 (n = 32) cultured hippocampal neurons. Analysis as in Figure 3A.

(B) Development of asymmetric dendritic arbors. Camera lucida drawings of MAP2-stained hippocampal neurons.

dendrite, which extends radially toward the pial surface. Staining for GM130 revealed that the Golgi apparatus of cortical pyramidal neurons extends into the proximal apical dendrite (Figure 3C). Such an extension was not observed in basolateral dendrites (data not shown). Quantitative analysis of Golgi orientation within the cell bodies of cortical pyramidal neurons showed a marked polarization of somatic Golgi toward the apical dendrite (Figure 3D). This orientation of the Golgi toward the apical dendrite resembles the orientation of somatic Golgi toward the longest dendrite in neurons in vitro (Figure 3E). Immunogold electron microscopy of hippocampal pyramidal neurons further demonstrated a selective concentration of GM130-labeled Golgi stacks at the exit zone of the apical dendrite (Figure 3F, left) but not in proximal basolateral dendrites (Figure 3F, right). Quantification of immunogold labeling for GM130 revealed a much higher density of labeling in proximal portions of apical dendrites than in basal dendrites (2.1 ± 0.3 versus 0.3 ± 0.1 particles/μm^2, $p < 0.001$) (Figure 3G). Finally, we examined the Golgi distribution in GABAergic interneurons. Unlike glutamatergic pyramidal neurons, these neurons lack apical dendrites and have dendrites of more uniform length. We observed a nearly symmetric distribution of somatic Golgi in GABAergic neurons compared to cocultured glutamatergic neurons (compare Figure 3H with Figure 3B), demonstrating that Golgi polarity correlates with dendrite polarity.

To determine whether Golgi polarization precedes and therefore predicts asymmetric dendritic growth, we examined the temporal relationship between Golgi polarization and dendritic outgrowth. We found that the polarized orientation of the somatic Golgi emerged as neurons differentiated in cell culture (Figures 3E and 4A) and preceded the appearance of dendritic asymmetry (Figure 4B). At DIV 5, neurons typically had several nearly equivalent dendrites (Figure 4B, left), and the Golgi in the soma concentrated near the longest of these dendrites (Figure 4A, left). By DIV 7, the mature polarized Golgi distribution was established (Figure 4A, middle), although the dendrites exhibited little polarity (Figure 4B, middle). By DIV 10, however, most neurons have clearly established a single longest dendrite (1°:2° dendrite ratio, 2.8 ± 0.3, n = 32) (Figure 4B, right), and the Golgi remained oriented to this longest dendrite (Figure 3C, shown again in Figure 4A, right, for ease of comparison).

Polarized Trafficking of Post-Golgi Cargo

To determine whether the polarized spatial distribution of neuronal Golgi predicts patterns of secretory flux, we performed time-lapse imaging of post-Golgi secretory trafficking in live neurons. For these experiments, we used a green fluorescent protein (GFP)-tagged temperature-sensitive mutant of the vesicular stomatitis virus glycoprotein VSVG-GFP-ts045, hereafter referred to as VSVG-GFP. VSVG-GFP misfolds and is retained in the ER when cells are incubated at the nonpermissive temperature (40°C). On shifting to a permissive temperature, VSVG-GFP folds properly, exits the ER, and proceeds to the Golgi. Thus, secretory cargo can be visualized as a synchronous wave. To accumulate VSVG-GFP in the Golgi after exit from the ER, we shifted neurons from

(F) Immunogold labeling for GM130 in adult rat hippocampus. In the soma of CA1 pyramidal neurons, GM130-labeled Golgi stacks were frequently located at the base and extending into the proximal apical dendrite (left, arrows). Immunogold labeling for GM130 is sparse or absent at the origin of basolateral dendrites (right). Scale bar, 0.5 μm. 0.25 μm, inset.

(G) Quantification of immunogold labeling for GM130 in the most proximal part of apical and basolateral dendrites of CA1 pyramidal neurons. Data represent particle density per μm^2. Data represent means ± SEM.

(H) Summation of images of the Golgi in the cell bodies of DIV 10 cultured GABAergic interneurons, aligned as in (A).

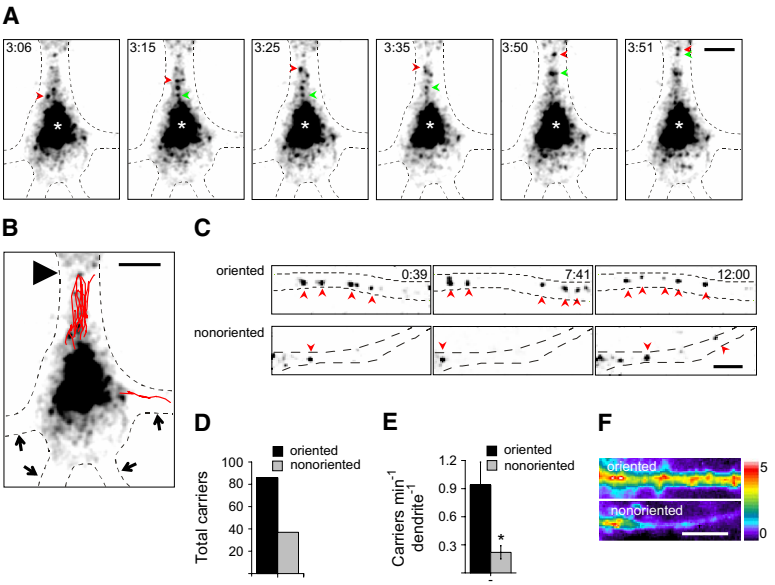

Figure 5. Post-Golgi Secretory Trafficking Is Preferentially Directed to a Single Dendrite

(A) Frames from a time-lapse imaging experiment show VSVG-GFP in the soma of a cultured hippocampal neuron (17 DIV) after incubation at 20ºC. VSVG-GFP accumulates in the somatic Golgi (white asterisk) and is also present in mobile carriers. Note the concentration of VSVG-GFP at 20ºC near the emergence point of one dendrite. The longest dendrite is up. Arrowheads indicate carriers proceeding from the somatic Golgi into the proximal dendrite. Frames are maximum intensity projections of z stacks acquired at 1.2 s intervals. Fluorescence is inverted so that fluorescent structures appear dark. Time is given in min:s after release from 20ºC blockade. Scale bar, 10 μm. See Movie S1 for complete time lapse.

(B) Post-Golgi carrier trajectories plotted on the proximal dendrites of a hippocampal neuron during the first 12 min after release from 20ºC block. The arrowhead indicates the proximal dendrite to which the somatic Golgi is oriented. Arrows indicate "nonoriented" dendrites. Each trajectory indicates a carrier that is trafficking in the anterograde direction, away from the neuronal soma. Of the 14 vesicles tracked, 13 entered the oriented dendrite apposed to the somatic Golgi. Scale bar, 10 μm.

(C) Representative frames from a Golgi-oriented and Golgi-nonoriented dendrite from the same hippocampal neuron expressing VSVG-GFP. At all time points examined after release from 20ºC, more post-Golgi carriers (arrowheads) are present in the oriented dendrite compared to the nonoriented dendrite. Time is indicated in min:s after release from 20ºC block. Scale bar, 5 μm. See Movies S2 and S3 for complete time lapse.

(D) Quantification of post-Golgi carriers in oriented and nonoriented dendrites. n = 123 carriers from 26 dendrites in five separate experiments.

(E) Cargo flux in oriented versus nonoriented dendrites, defined as the total carriers per dendrite per minute. Asterisk, $p < 0.05$. Data represent means ± SEM.

(F) Summed images from 600 frames of a time-lapse experiment over a 15 min period after release from 20ºC block. Regions shown are of an oriented and nonoriented dendrite from the same neuron. Scaled pseudocolor fluorescence intensities represent contributions from all post-Golgi carriers containing VSVG-GFP present in these dendritic segments over the entire time course of the experiment. Scale bar, 10 μm.

40ºC to 20ºC, a temperature that allows VSVG-GFP to escape the ER, but inhibits budding from the Golgi (Matlin and Simons, 1983). After a 3 hr incubation at 20ºC, VSVG-GFP was present predominantly in the neuronal soma, where it colocalized with GM130 (Figure S3), and also in puncta throughout the dendrites.

After the 20ºC incubation, neurons were imaged live at 32ºC, a temperature at which post-Golgi trafficking is restored (Yeaman et al., 2004). Under these conditions, post-Golgi trafficking of VSVG-GFP-labeled carriers was readily observed (Movies S1 and S2). We found that VSVG-GFP was present in highly mobile carriers in the neuronal soma, as well as the proximal and distal dendrites, at all time points after release from the 20ºC block. Post-Golgi traffic was particularly dense in the proximal dendrites, where individual vesicles were frequently observed moving from the neuronal soma outward into the dendrites (Figure 5A, arrowheads, and Movie S1). Consistent with our immunostaining for GM130 (Figures 3A and 3B), Golgi labeled by VSVG-GFP after 20ºC block typically localized to the base of a single long dendrite (Figure 5A and data not shown). In our time-lapse experiments, we designated the dendrite emerging nearest the Golgi as the "oriented" dendrite and other dendrites as "nonoriented" dendrites. At a distance of 40 μm from the cell body, there was no difference in the width of oriented versus nonoriented dendrites (2.1 ± 0.1 versus 1.8 ± 0.1 μm, $p > 0.05$). Upon exit from the Golgi, carriers preferentially entered the oriented dendrite (Figure 5B). Even in more distal dendritic segments, post-Golgi carriers were consistently more numerous in the oriented dendrites at all time points following release from 20ºC block (Figure 5C, arrowheads, and Figure 5D; see also Movies S2 and S3). This includes both anterograde (70%) and retrograde (30%) trafficking carriers. This count of total carriers likely underestimates the bias of post-Golgi traffic for the oriented dendrite because each neuron typically has only a single oriented dendrite and several nonoriented dendrites. Therefore, we normalized the total number of vesicles to the number of dendrites in each group and found a 4-fold greater secretory flux in oriented dendrites (Figure 5E). To corroborate these findings, we summed 600 frames of individual time-lapse experiments and observed an approximately 5-fold greater flux of VSVG-GFP in Golgi-oriented dendrites, relative to nonoriented dendrites (Figure 5F). These results demonstrate that post-Golgi secretory trafficking in hippocampal neurons is directed predominantly toward a single principal dendrite, supporting our hypothesis that the polarized spatial orientation of the Golgi leads to polarized secretory trafficking.

Golgi Outposts at Dendritic Branchpoints

The delivery of cargo for dendrite growth and maintenance requires navigation through the highly branched dendritic tree. Given the relationship between Golgi polarization and dendritic complexity (Figure 2), we hypothesized that Golgi structures in dendrites would be positioned to regulate protein sorting and membrane addition associated with the development of complex dendrites. To test this possibility, we used 20ºC block of VSVG-GFP to accumulate and visualize labeled secretory

cargo in the Golgi and TGN. We found that Golgi outposts are frequently located at dendritic branchpoints (Figures 6A and 6B). VSVG-GFP-labeled stable Golgi structures were present at the majority of 1° and 2° dendritic branches, as well as nearly 40% of 3° dendrites (Figures 6B and 6C). A comparison of the distribution of distances between Golgi elements and dendritic branchpoints, the distribution of distances between individual Golgi outposts, and the distribution of distances between branchpoints, revealed a strong bias for dendritic Golgi to appear at branch bifurcations (Figure 6D). Although outposts were not completely restricted to branchpoints (Table 1), outposts at branches were located in close proximity to the branch bifurcation, even in distal dendrites (Figure 6E). Immunogold labeling for GM130 in cortical pyramidal neurons revealed Golgi stacks at dendritic branches in vivo, with the trans face oriented for cargo delivery into the opposing branch (Figure 6F). Thus, Golgi outposts are positioned to accommodate dendritic sorting and trafficking between dendritic branches.

To gain a better understanding of the behavior of secretory trafficking at branchpoints, we performed time-lapse imaging experiments of post-Golgi secretory cargo by visualizing VSVG-GFP in dendrites (Movie S4). After release from 20°C block, VSVG-GFP collected in stable, stationary structures at branchpoints (Figure 6G). These stationary Golgi structures were distinct from the smaller mobile post-Golgi carriers that trafficked bidirectionally throughout the dendrites with velocities of 1.0 ± 0.1 μm/sec (Figure 6G). Kymograph analysis confirmed the immobile behavior of branchpoint Golgi (Figure 6H). In these traces, the stable Golgi elements appeared as thick, straight lines (Figure 6H, colored arrows), indicating an accumulation of VSVG-GFP that has not yet budded into the more mobile post-Golgi vesicles, which appeared as the thinner sloped dotted lines across the kymograph (black arrows). Small carriers of post-Golgi cargo were frequently observed to traffic between these stable Golgi elements (Figure 6G) and to bud from them (Figures 6I and 6J and Movie S5). Although secretory cargo exiting from somatic Golgi showed a clear bias toward entering the nearby "oriented" dendrites (Figure 5), we did not discern a similar bias for cargo to enter a particular dendritic branch. For example, in the experiment shown in Figures 6G and 6H, a vesicle entered branch B (green arrowheads) shortly after another vesicle trafficked into branch A (red arrowheads). We conclude that stable Golgi elements engaged in secretory trafficking reside at most dendritic branchpoints. These Golgi sorting stations provide an intracellular landmark of dendritic branching and suggest a role for post-Golgi trafficking in regulating dendrite complexity and controlling the transport of molecular components to specific dendrite branches.

Requirement for Forward Secretory Trafficking in Dendritic Outgrowth

The above data show a strong correspondence and sequential temporal relationship between a polarized Golgi distribution, polarized secretory trafficking, and enhanced dendritic length and complexity, suggesting a causal relationship. To determine whether forward secretory trafficking is required for dendritic outgrowth, we inhibited secretory trafficking by treating developing neurons with brefeldin A (BFA), which reversibly disassembles the Golgi apparatus (Lippincott-Schwartz et al., 1989). In dissociated culture, developing neurons progress from stage 3, with a single specified axon and nascent neurites, to stage 4, with clearly differentiated dendrites that stain for MAP2. In our system, this period of dramatic dendritic outgrowth occurred during the 24 hr between 2 and 3 DIV (from 25.5 ± 7.8 to 169.9 ± 22.8 μm total dendritic outgrowth per neuron), a period before polarization of the dendritic arbor and before polarization of the Golgi. We selected this period to investigate whether secretory trafficking contributes to the initial formation and growth of dendrites. Including BFA (1 μg/ml) in the growth medium during this period inhibited dendritic outgrowth by 86% (control, 169.9 ± 22.8 μm total dendrite length; BFA, 45 ± 7.4; n = 25, 20, $p < 0.001$) (Figures 7A–7C). A normal rate of dendritic growth resumed within 48 hr of drug washout (Figures 7A–7C). A similar effect was observed when 2 DIV neurons were treated with 1,3-cyclohexanebis(methylamine) (CBM, 1 mM, 24 hr), an inhibitor of COPI that blocks ER-to-Golgi trafficking by binding to coatomer (Hu et al., 1999) (Figure 7C).

To determine whether forward secretory trafficking was required for the maintenance of dendritic arbors that have achieved mature morphology, we treated mature neurons (22 DIV) with BFA (1 μg/ml, 24 hr). We found an average loss of more than 600 μm of total dendritic length (29%) after 24 hr treatment with BFA (BFA, 1559 ± 223 μm; control, 2216 ± 208 μm; n = 11, 17; $p < 0.05$) (Figure 7D). Treatment with BFA and CBM had no effect on cell viability, as determined by trypan blue exclusion (98.8% ± 4% exclusion by control cells; 88.3% ± 6%, BFA; 96.4% ± 1%, CBM), and emphasized by the reversibility of the observed effects and the continued growth of cells for up to 3 weeks after drug treatment (data not shown).

As a complement to pharmacological blockade of Golgi trafficking, we tested the effect of more selective inhibition by expressing dominant-inhibitory secretory pathway regulatory proteins. For this approach, we used a kinase-dead (KD) mutant of protein kinase D1 (PKD1-K618N, referred to here as PKD-KD), which blocks late secretory trafficking by preventing cargo budding from the TGN (Liljedahl et al., 2001). Expression of PKD-KD in 2 DIV neurons caused a decrease in total dendritic outgrowth that was evident by 3 DIV (PKD-KD, 115.1 ± 18 μm total dendrite length, n = 20; control, 175.6 ± 21.2 μm; n = 28, $p < 0.05$) (Figures 7A and 7E) and persisted over the next 48 hr (Figure 7E). Similar suppression of dendritic growth was observed in neurons expressing Arf1-Q71L, a GTPase-deficient mutant of the Arf1 small GTPase that blocks secretory trafficking by causing secretory cargo to accumulate in pre-Golgi intermediate vesicles (Dascher and Balch, 1994) (Figures 7A and 7E).

To test whether forward secretory trafficking is required for dendritic outgrowth in more physiological neural circuits, we expressed PKD-KD in layer IV–V pyramidal neurons in organotypic cortical slice cultures from 15-day-old mice. Cell morphology was determined by expression of mRFP or GFP, and dendritic arbors were reconstructed and analyzed from confocal stacks.

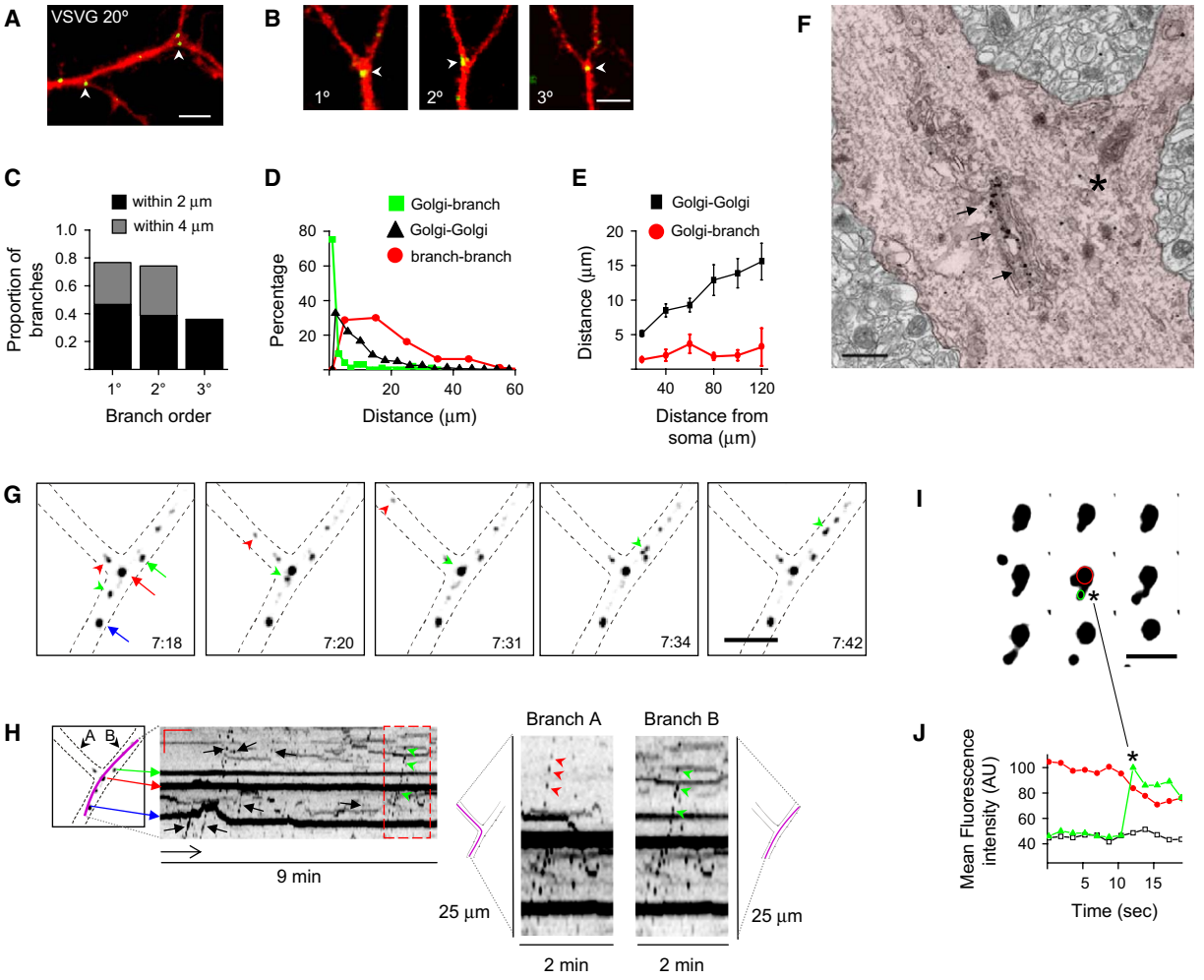

Figure 6. Golgi and Post-Golgi Elements Accumulate at Dendritic Branchpoints

(A) Dendrite of a hippocampal neuron (16 DIV) expressing VSVG-GFP (green) and mRFP (red) after incubation at 20ºC to accumulate VSVG-GFP in the Golgi. VSVG-GFP is present in discrete puncta, frequently located at dendritic branchpoints (arrowheads). Scale bar, 5 μm.

(B) Examples of VSVG-GFP (green) accumulation in dendritic Golgi (arrowheads) at primary (1º), secondary (2º), and tertiary (3º) branchpoints after incubation at 20ºC. Scale bar, 5 μm.

(C) Proportion of dendritic branchpoints with dendritic Golgi. n = 91 branchpoints from 11 neurons.

(D) Normalized distribution of the distances between dendritic Golgi and branchpoints (green squares, 97 observations), between individual Golgi outposts (black triangles, 312 observations), and between individual dendritic branches (red circles, 80 observations).

(E) A plot of inter-Golgi intervals (black squares) and Golgi-branchpoint distances (red circles) as a function of linear distance from the neuronal soma. n = 312 Golgi outposts in 12 neurons, marked by VSVG-GFP accumulation at 20ºC. Data represent means ± SEM.

(F) Immunogold labeling for GM130 in the apical dendrite of a pyramidal neuron in adult rat somatosensory cortex shows a dendritic branch (asterisk) with a nearby GM130-labeled Golgi stack (arrows). Scale bar, 0.5 μm.

(G) Post-Golgi trafficking at dendritic branchpoints. Frames from a time-lapse imaging experiment showing VSVG-GFP in dendritic puncta after incubation at 20ºC and switch to 32ºC. Three puncta (arrows) are located in the vicinity of the dendritic branch, including one immediately at the point of bifurcation (red arrow). These puncta are stable and stationary over the course of the experiment, in contrast to the smaller, more highly mobile vesicles (arrowheads) that traffic into each dendritic branch. Fluorescence has been inverted such that fluorescent structures appear dark. Time is given in min:s after switch to 32ºC to release cargo from the Golgi. Scale bar, 10 μm. See Movie S4 for complete time lapse.

(H) Kymograph of a linear region drawn along the dendritic branch indicated by the magenta line. Stable dendritic Golgi outposts appear as the corresponding straight, solid black horizontal lines in the kymograph. Arrows are color coded to indicate which line corresponds to each Golgi puncta labeled in (G). Stable Golgi are present throughout the duration of the 9 min experiment (colored arrows on solid lines), in sharp contrast to the smaller, sloped traces of mobile secretory carriers (black arrows). Horizontal scale bar, 1 min. Vertical scale bar, 5 μm. The dashed red box indicates the 2 min segment of the kymograph that is shown in the right panels for each dendritic branch. This 2 min segment corresponds to the frames shown in (G). In these expanded kymographs, red and green arrowheads indicate the trajectories of the two moving carriers entering branch A and branch B, respectively, as indicated in (G).

(I) Cargo budding from Golgi at a branchpoint. A carrier (green circle) buds from a stable Golgi element (red circle) and moves along the dendrite. Images are from the same time lapse as in (G). Scale bar, 1 μm. See Movie S5 for complete time lapse.

(J) Total fluorescence intensities of two small regions overlying the Golgi (green triangles) and budding carrier (red circles) shown in (H) and of the mean intensity of a region encompassing both spots (white squares). The asterisk indicates the time on the graph corresponding to the indicated frame in (H). AU, arbitrary units.

Table 1. Spatial Distribution of Dendritic Golgi Outposts

	Distance from Soma (μm)					
	20	40	60	80	100	>120
% Golgi outposts at branches	55 ± 13	34 ± 13	29 ± 11	38 ± 13	31 ± 15	31 ± 14

The percentage of Golgi outposts within 2 μm of a dendritic branchpoint is shown as a function of distance from the soma.

Control neurons expressing RFP alone exhibited typical elaborate dendritic arbors with prominent apical dendrites (Figure 7F, top panels). In contrast, examination of adjacent neurons in the same slices expressing PKD-KD and GFP showed that cortical pyramidal neurons expressing PKD-KD (24–48 hr) possessed shorter and simpler dendrites (Figure 7F, bottom panels). Sholl analysis revealed a marked reduction in dendritic length and complexity in neurons expressing PKD-KD (Figure 7G) (see Experimental Procedures for details). Quantitatively, we found a 51% decrease in apical dendritic length in pyramidal neurons transfected with PKD-KD (PKD, 338.2 ± 69.9 μm; control 695.5 ± 81.2 μm, n = 15 cells per group, $p < 0.005$) (Figure 7H). Further, expression of PKD-KD caused a 3-fold reduction in branch number of the apical dendrite, relative to control neurons (1.5 ± 0.3 versus 4.6 ± 1.1) (Figure 7I). Taken together, these results support the conclusion that PKD- and Arf1-dependent secretory trafficking is required for the growth, initiation, and maintenance of dendrites.

Golgi Polarity Is Required for Asymmetric Dendritic Growth

To directly test the hypothesis that Golgi polarization is required for enhanced growth of the principal dendrite, we sought a manipulation that disrupted Golgi organization without affecting secretory function per se. We found that overexpression of the Golgi structural protein GRASP65-GFP (Barr et al., 1997) caused Golgi vesiculation and dispersal into multiple dendrites (Figure 8A), without inhibiting secretory function (Figure S4). Expression of GRASP65-GFP between DIV 8 and DIV 10, a period of asymmetric dendrite growth (Figure 4B), resulted in a marked reduction in dendrite polarity (1° to 2° dendrite length ratio: 3.4 ± 0.8, control; 1.5 ± 0.1, GRASP65, $p < 0.02$) (Figures 8B and 8C). Unlike global secretory inhibition (Figure 7), GRASP65-GFP overexpression did not result in a decrease in total dendritic outgrowth (982 ± 87 versus 803 ± 58, $p > 0.05$) (Figure 8D), indicating that secretory trafficking supporting overall dendrite growth remained intact. Thus, polarized dendritic growth requires a spatially polarized Golgi.

Golgi Is Not Polarized toward the Axon

Axonal outgrowth also requires membrane addition (Jareb and Banker, 1997); therefore, if Golgi polarity and the directionality of post-Golgi trafficking were simply a "passive" response to the need for more membrane, one might expect the Golgi to be polarized toward the axon during periods of rapid axonal outgrowth. Surprisingly, this was not the case (Figure 9). Golgi outposts labeled by VSVG-GFP after 20ºC incubation, which were frequently observed in dendrites (Figure 6 and Figure 9A, arrowheads), were not observed in axons, even in proximal regions very close to the neuronal soma (Figure 9A, left, arrow). Similarly, Golgi in the neuronal soma had no spatial relationship to the axon, either at very early stages of development during axon specification (Figure 9B) or at subsequent time points (Figures 9C and 9D).

Finally, we found that blockade of post-Golgi trafficking by expression of PKD-KD had a delayed effect on axonal outgrowth (Figure 9E). Although dendritic outgrowth was rapidly suppressed upon expression of PKD-KD (Figure 7E), we found no effect on axons of the same neurons at 3 DIV (PKD-KD, 210.6 ± 33.0 μm, n = 20; control, 278.5 ± 33.4 μm; n = 28, $p > 0.05$) (Figures 9E and 9F). Further, these axons continued to grow normally from 3 to 4 DIV, even as dendrite growth was arrested (Figures 7E and 9F). These data show that axonal outgrowth can temporarily persist despite post-Golgi secretory blockade, demonstrating a selective role for polarized secretory trafficking in dendritic, but not axonal, outgrowth.

Discussion

Anterograde Secretory Trafficking as a Mechanism for Dendritic Polarity

We have described a novel role for polarized anterograde secretory trafficking in the formation of asymmetric dendritic arbors of pyramidal neurons (Figure S5). This polarized trafficking is evident in the polarized organization of the neuronal Golgi apparatus, both in dendrites and in the soma. Dendritic Golgi outposts are found only in the longest and most complex dendrites where they localize at dendritic branchpoints. Within the cell body, the Golgi apparatus is polarized toward the single longest dendrite in culture and the apical dendrite in pyramidal neurons in vivo. This distribution of Golgi predicts the directionality of anterograde secretory flux because post-Golgi secretory cargo preferentially traffics into dendrites adjacent to somatic Golgi. In the absence of post-Golgi membrane trafficking, dendrites rapidly shrink and simplify. Importantly, during development, Golgi polarization precedes enhanced growth of the principal dendrite, and disruption of Golgi polarity leads to more symmetric dendritic growth. This role for polarized secretory trafficking is specific to dendrites because axons lack Golgi outposts and continue to grow even in the presence of inhibitory mutants that block post-Golgi trafficking. GABAergic neurons lacking highly polarized dendritic arbors lack polarized Golgi. Further, no other organelle system exhibits polarization to a single dendrite. Together, these data define an unanticipated organization of the neuronal secretory machinery and reveal a direct role for spatially oriented secretory trafficking in the asymmetric growth of pyramidal neuron dendrites.

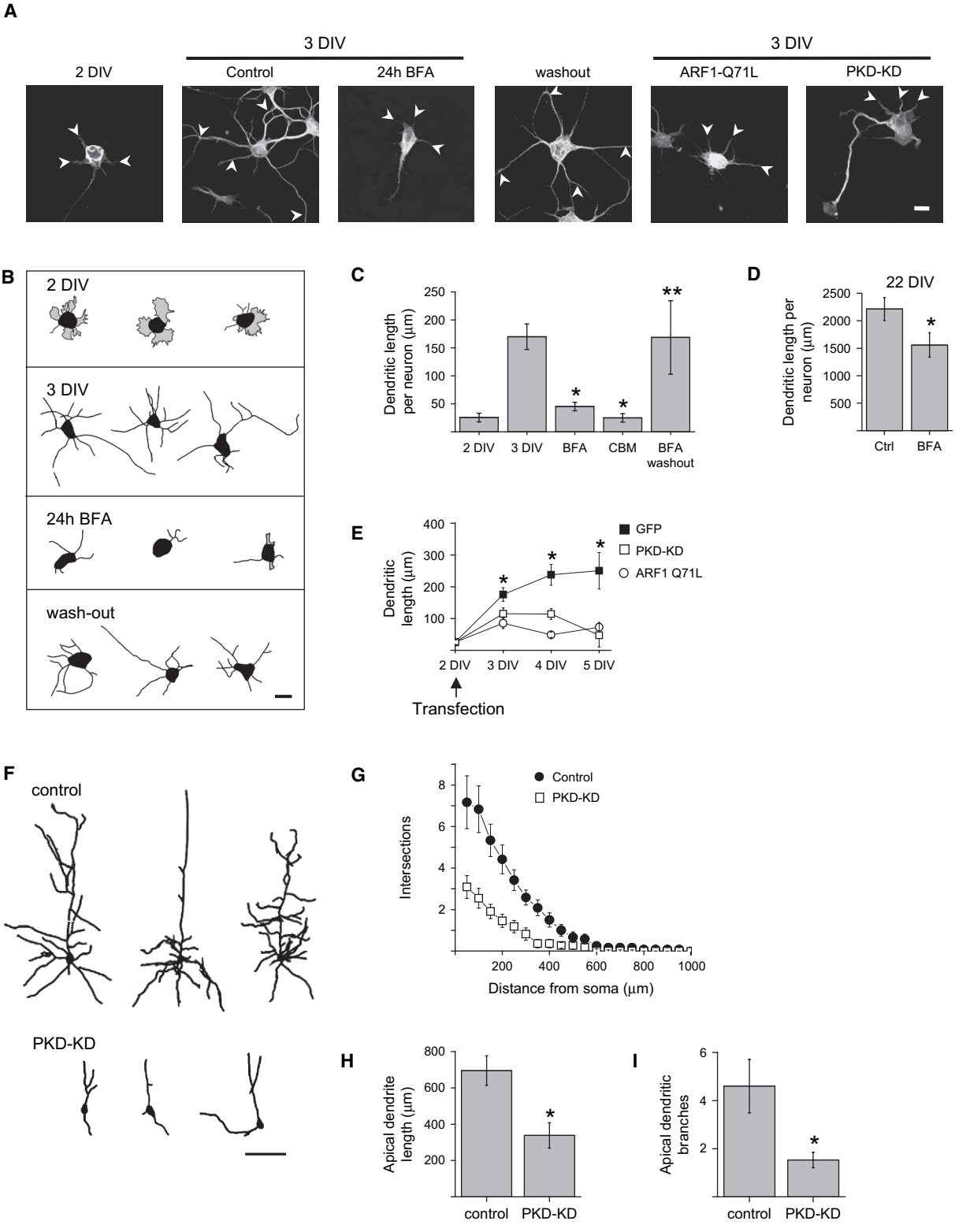

Figure 7. Forward Secretory Trafficking Is Required for Dendritic Outgrowth

(A) Hippocampal neurons expressing EGFP alone (first four panels) or EGFP together with ARF1-Q71L or PKD-KD (right two panels) and stained for MAP2. At DIV 2, neurons have a single specified axon and a number of short neurites (left, arrowheads). By DIV 3, neurons have much longer dendrites that stain strongly for MAP2 (control, arrowheads). Addition of BFA between DIV 2 and 3 prevents the elaboration of MAP2-positive dendrites (arrowheads). Normal dendritic outgrowth is restored after BFA washout. Expression of PKD-KD or ARF1-Q71L for 24 hr reduces total dendritic outgrowth. Scale bar, 10 μm.

(B) Camera lucida drawings of 2 and 3 DIV control neurons, as well as BFA-treated 3 DIV neurons and 5 DIV neurons 48 hr after BFA washout. Only MAP2-positive processes were traced. Scale bar, 20 μm.

Regulation of Golgi Distribution and Dendrite Morphology

An important aspect of the present work is our observation that disruption of Golgi organization, through overexpression of the Golgi matrix protein GRASP65 (Barr et al., 1997), inhibits polarized dendritic outgrowth without affecting total dendritic length. This result implies a mechanistic relationship between Golgi organization and polarized dendrite growth and implicates the Golgi matrix as a potential regulatory target for controlling neuronal morphology. GRASP65, a peripheral membrane protein important for cisternal stacking (Barr et al., 1997), has previously been shown to regulate Golgi fragmentation during mitosis (Lin et al., 2000) and apoptosis (Lane et al., 2002). GRASP65 exists in a complex with the tethering proteins GM130 and p115 (Shorter and Warren, 1999), and proper stoichiometry of these interactions is necessary for normal Golgi structure. GRASP65, one of the main phosphoproteins at the Golgi (Barr et al., 1997), is targeted by numerous kinase signaling pathways (Lin et al., 2000). Intriguingly, GRASP65 has also been implicated as a target of ERK signaling downstream of extracellular growth factors in interphase cells (Yoshimura et al., 2005), directly linking GRASP65 phosphorylation, Golgi organization, and cellular growth programs in nonneuronal cells.

A second Golgi protein identified in this study as a potential regulator of neuronal development is protein kinase D (PKD). We used expression of a kinase-dead protein kinase D1 mutant (PKD-KD) to test directly whether post-Golgi secretory trafficking is necessary for dendritic outgrowth. PKD is a serine/threonine protein kinase that acts at the TGN, where it regulates the fission of post-Golgi carriers for the plasma membrane via a mechanism requiring its kinase activity (Liljedahl et al., 2001). Unlike drugs such as BFA, which can also affect membrane recycling through the endocytic pathway, PKD-KD acts as a selective block of the anterograde secretory pathway (Liljedahl et al., 2001; Yeaman et al., 2004), and PKD inhibition has been used to demonstrate a requirement for polarized anterograde secretory trafficking in cell migration (Prigozhina and Waterman-Storer, 2004). Although these experiments are the first direct evidence that PKD activity is required in neuronal morphogenesis, it is interesting that overexpression of PKCε, which activates PKD (Waldron and Rozengurt, 2003), stimulates neurite outgrowth in neuronal cell lines (Brodie et al., 1999). Moreover, PKD activation is controlled by the synchronized actions of PKC and PKA via the anchoring protein AKAP-Lbc (Carnegie et al., 2004), raising the possibility that kinase signaling pathways regulate PKD-dependent trafficking in dendrites.

Polarized Delivery of Cargo to Neuronal Dendrites

Previous work has shown that the exocyst complex controls the local insertion of membrane required for neurite outgrowth (Murthy et al., 2003), but the source of membrane and the route by which it reaches insertion sites have remained obscure. Here, we have shown a preference for post-Golgi cargo to enter dendrites closest to the Golgi apparatus. This pattern of secretory flux is consistent with a growing body of evidence indicating that some proteins eventually localized to the axon or axon initial segment are first preferentially inserted into the somatodendritic membrane (Fache et al., 2004; Sampo et al., 2003; Wisco et al., 2003). In some cases, these proteins are then internalized and targeted to the axon or axon initial segment by transcytosis (Sampo et al., 2003; Wisco et al., 2003). Given the differential effects on axonal versus dendritic outgrowth on post-Golgi blockade by PKD-KD expression (Figures 7 and 9), one possibility is that this endosomal delivery of membrane is sufficient to maintain axonal outgrowth even in the absence of on-going secretory trafficking. As endosomes are distributed throughout the dendritic arbor (Figure S1 and data not shown), ongoing endocytic trafficking could explain the observed shrinkage and simplification of all dendrites in the presence of secretory pathway blockade (Figure 7).

Molecular Composition of Golgi Outposts

We previously described the location and function of atypical Golgi-like structures in neuronal dendrites (Horton and Ehlers, 2003). These structures are similar to somatic Golgi in that both are composed of stacks of cisternal membranes (Figure 1), both possess Golgi tethering proteins and resident enzymes, and both receive secretory cargo. In our experiments, Golgi stacks were always located along the dendritic shafts in vivo and had little colocalization with synaptic markers in vitro (Horton and Ehlers, 2003). However, other groups have reported labeling for Golgi proteins at synapses and within dendritic spines (Gardiol et al., 1999; Pierce et al., 2001). TGN-derived organelles have also been reported to be associated with neural cell adhesion molecule in developing dendrites, where they deliver cargo for synaptogenesis (Sytnyk et al., 2002). Immunogold labeling experiments have revealed Golgi proteins on

(C) Quantification of total dendritic length per neuron. n = 7 to 27 neurons in each group. Comparisons were BFA and 1,3-cyclohexanebis(methylamine) (CBM) groups versus 3 DIV control group and BFA washout versus BFA. Asterisk, $p < 0.001$; double asterisk, $p < 0.005$. Data represent means ± SEM.

(D) Quantification of total dendritic length per neuron on DIV 22 hippocampal neurons under control conditions (Ctrl) or after 24 hr BFA treatment. n = 17 (control) and 11 (BFA) neurons. Asterisk, $p < 0.05$. Data represent means ± SEM.

(E) Quantification of total dendritic length as a function of duration of expression of the indicated constructs. Asterisks indicates significant differences between GFP control and both PKD-KD and ARF1-Q71L groups. n = 10 to 28 neurons in each group. Asterisk, $p < 0.05$. Data represent means ± SEM.

(F) Camera lucida drawings of layer IV/V pyramidal neurons in cortical slices cultured from P15 mice and transfected via biolistics with mRFP alone (control) or EGFP and PKD-KD. Constructs were expressed for 48 hr. Scale bar, 50 μm.

(G) Sholl analysis for mRFP transfected (n = 15, black circles, control) and EGFP and PKD-KD cotransfected neurons (n = 15, white squares). See Experimental Procedures for details. Data represent means ± SEM.

(H) The length of apical dendrites is reduced by expression of PKD-KD. n = 15 neurons in each group; asterisk, $p < 0.005$. Data represent means ± SEM.

(I) The number of apical dendritic branches is reduced by expression of PKD-KD. n = 15 neurons in each group; asterisk, $p < 0.05$. Data represent means ± SEM.

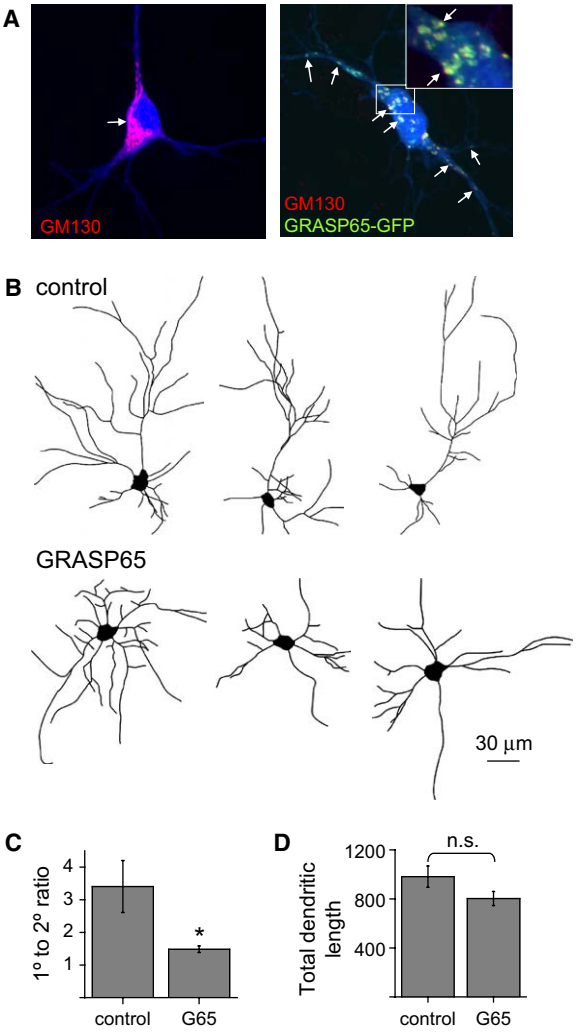

Figure 8. Disruption of Golgi Polarity Results in Uniform Dendritic Growth

(A) Golgi in a control neuron (10 DIV) (left) is polarized toward a dendritic origin (arrow). In a hippocampal neuron (10 DIV) overexpressing GRASP65-GFP (right), the somatic Golgi becomes vesiculated (inset), and Golgi fragments are present in multiple dendrites (arrows).

(B) Camera lucida drawings of control neurons, expressing GFP, and neurons overexpressing GRASP65-GFP. Control neurons have polarized dendritic arbors, whereas neurons overexpressing GRASP65 do not.

(C) Polarity index (ratio of 1° to 2° dendritic lengths) of control neurons and neurons overexpressing GRASP65-GFP. n = 21 (control), 23 (GRASP-65); asterisk, $p < 0.02$. Data represent means ± SEM.

(D) Total dendritic length is unaffected by GRASP65-GFP. n = 21 (control), 23 (GRASP-65); n.s., not significant. Data represent means ± SEM.

amorphous membranous structures in dendritic spines (Pierce et al., 2001), leaving open the question whether multiple types of Golgi-like structures function in dendrites. One possibility is that these spinous structures were below the limits of resolution of the light microscopic techniques we employed. However, the use of molecular markers to identify the Golgi is complicated by the fact that Golgi membranes cycle continuously between the ER and *cis*-Golgi (Lippincott-Schwartz et al., 1989), and between the trans-Golgi and endosomes (Mallard et al., 1998), introducing ambiguity into the interpretation of steady-state immunogold labeling in the absence of functional data and dynamic visualization. Additionally, neurons have other atypical membrane bound organelles, such as the extension of smooth ER into spines, the spine apparatus (Spacek and Harris, 1997), and cisternal organelles that function in calcium signaling in the axon initial segment. The Golgi outposts we describe are distinct from these organelles, in that they do not appear in spines or the axon. Clearly, however, the numerous specialized neuronal endomembranes await a more thorough molecular characterization.

Forward Secretory Trafficking and Dendritic Complexity

Formation of dendritic branches requires redirection of membrane, the basis of which has been almost completely unknown. First principles of cell geometry argue for the need to sort cargo at branchpoints, but the cellular machinery conducting this sorting is enigmatic. Here, we have shown a tight correlation between the presence of dendritic Golgi and enhanced dendritic branching. VSVG-GFP-labeled post-Golgi elements and morphological Golgi stacks localize at dendritic branchpoints, where they flux cargo. The majority of primary and secondary branchpoints have an associated Golgi structure at the bifurcation, and dendritic Golgi are preferentially located at branchpoints. The spatial distribution of these post-Golgi elements suggests a role in establishing or maintaining dendritic complexity. Live imaging of highly arborized neurons in *Drosophila* and zebrafish has revealed that dendritic outgrowth and branching are dynamic processes, with dendritic branches extending and retracting as dendrites undergo remodeling (Jontes et al., 2000; Niell et al., 2004). Although the source of membrane components necessary for building or maintaining new dendritic branches was not examined in these studies, Golgi at branchpoints would be ideally positioned for the role.

In addition to supplying the membrane components required for surface expansion, secretory trafficking directs the delivery of integral membrane proteins and the release of growth factors needed to support localized signaling. Results presented here support a direct link between the spatial organization of secretory traffic and localized delivery of molecular cargo. Our findings suggest that local Golgi-derived transport directs cargo toward preferred destinations, perhaps in response to local signaling events. TGN-derived elements have been shown to undergo calcium-evoked exocytosis in dendrites (Maletic-Savatic and Malinow, 1998), where they deliver cargo for synaptogenesis (Sytnyk et al., 2002). Transmembrane signaling proteins and adhesion molecules involved in the formation of synapses and in dendritic outgrowth and branching (Hoogenraad et al., 2005) must all be transported through the secretory pathway. The synthesis and membrane insertion of AMPA-type glutamate receptors occurs locally in dendrites in response to plasticity-inducing stimuli (Ju et al., 2004), implying dendritic localization of all requisite organelles of the secretory pathway in at least some dendrites (Horton and Ehlers, 2004). Finally, it is well established that locally released growth factors, such as neurotrophins, modulate dendritic branching patterns (Horch and Katz, 2002; McAllister et al., 1997). Interestingly, the

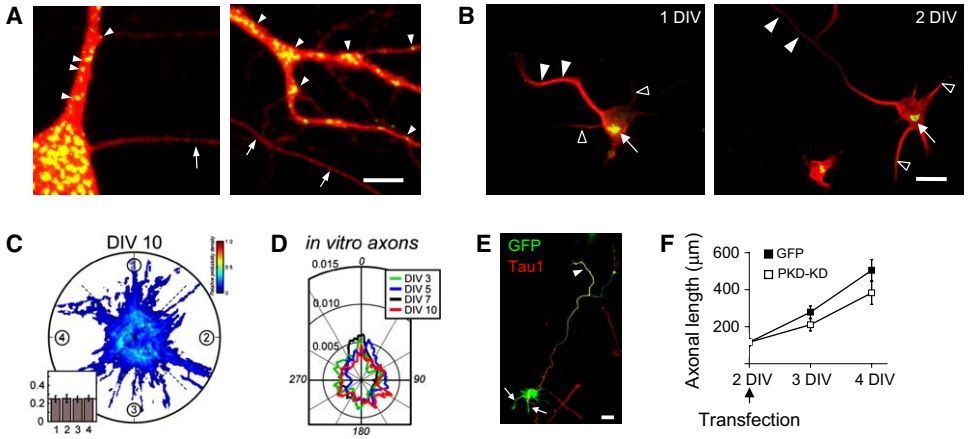

Figure 9. Golgi Is Not Polarized toward the Axon

(A) Hippocampal neurons (16 DIV) expressing VSVG-GFP (green) and mRFP (red) after incubation at 20ºC. VSVG-GFP is present in the neuronal soma and in discrete puncta in the proximal (left) and distal (right) dendrites (arrowheads) but is absent from the proximal and distal axons (arrows). Scale bar, 5 μm.

(B) Hippocampal neurons (red) stained for GM130 (green) at indicated ages. The Golgi (arrow) is not located adjacent to the longest neurite (arrowheads), which is destined to become the axon. Open arrowheads, nascent dendrites.

(C) Summation of GM130-labeled Golgi images in 10 DIV (n = 32) cultured hippocampal neurons aligned as in Figure 3A, except with the axon at 0º. Pseudocolor scale for summed fluorescence intensity is shown at right. The inset bar graph shows the fraction of fluorescence present in each quadrant.

(D) Cumulative angular probability distributions of Golgi fluorescence in neurons at 3 DIV (n = 26), 5 DIV (n = 25), 7 DIV (n = 25), and 10 DIV (n = 32) indicate a random distribution with respect to the axon in primary neuron cultures. Angles are defined as in (C).

(E) Hippocampal neuron (3 DIV) expressing PKD-KD and EGFP and stained for tau-1 (red). PKD-KD expression inhibits the outgrowth of dendrites (arrowheads) but not the axon (arrow). Scale bar, 10 μm.

(F) Quantification of axonal length as a function of duration of expression of the indicated constructs. n = 20 (PKD-KD) and 28 (GFP) neurons in each group. $p > 0.05$.

neurotrophin BDNF traffics through dendritic Golgi in hippocampal neurons (Horton and Ehlers, 2003), raising the possibility that local regulation of the secretion of these growth factors or their receptors could influence dendritic branching patterns in an autocrine fashion. We propose dual roles for the Golgi in promoting dendritic outgrowth whereby post-Golgi transport delivers the structural components necessary to build dendrites and synapses while delivering the signaling molecules required to coordinate extracellular signaling, synaptogenesis, and dendrite formation.

Membrane Trafficking and Apical Dendrite Specification

An extended apical dendrite is a cardinal feature of cortical and hippocampal circuitry. Here, we have shown that neuronal Golgi extends selectively into the apical dendrites of pyramidal neurons in the cortex and hippocampus and that dendritic Golgi stacks are a feature of apical dendrites. This spatial distribution, together with our results showing a requirement for post-Golgi trafficking in maintaining the length and complexity of the apical dendrite, indicates that polarized anterograde secretory trafficking is a central feature of apical dendrite formation and confers an internal dendritic polarity. The oriented growth of apical dendrites toward the pial surface is directed by the diffusible chemoattractant semaphorin 3A (Sema3A) (Polleux et al., 2000). Polarized secretory trafficking may create the polarized distribution of signaling molecules such as guanylyl cyclase (Polleux et al., 2000), plexin receptors, or the neuropilin-1 receptor necessary for Sema3A signaling. Alternatively, Golgi distribution and anterograde secretory trafficking may be regulated downstream of Sema3A, perhaps via rapid signal-dependent regulation of the Golgi matrix (Yoshimura et al., 2005) or via transcriptional events (Hand et al., 2005). More broadly, spatial control over the organization of secretory trafficking may provide a general mechanism for elaborating dendrites in diverse neural circuits.

Experimental Procedures

DNA constructs, antibodies, tissue culture, and immunocytochemistry methods are included in the Supplemental Data.

Live Cell Imaging

Time-lapse imaging of live neurons and confocal microscopy was performed as previously described (Horton and Ehlers, 2003) with minor variations. See Supplemental Data.

Immunogold Electron Microscopy

Immunogold labeling of brain sections from adult (3–5 months old) male Sprague-Dawley rats from Charles River (Raleigh, NC) was performed with anti-GM130 antibody (BD Transduction Laboratories). Detailed methods are provided in the Supplemental Data.

Quantitative Analysis of the Immunogold Reaction

Electron micrographs were taken from randomly selected fields, focusing on CA1 stratum pyramidale, and proximal stratum radiatum and stratum oriens, extending out to ~50 μm from the cell body layer. To determine relative densities of GM130 labeling, we identified dendrites, cell bodies, and pyramidal cell nuclei; gold particles within their cytoplasm were counted, and areas measured. Both labeled and unlabeled profiles were included in the analysis. To determine background, we calculated labeling over pyramidal cell nuclei (because nuclei did not stain for GM130 in LM material). Membrane

perimeters and profile areas were measured with the area calculator plugin of ImageJ v1.29 software (NIH; for further information, see http://rsb.info.nih.gov/ij/plugins/area.html).

Image Analysis

All processing for somatic Golgi orientation was performed in Matlab (R13—The MathWorks, Inc., Natick, MA). Masks were created by intensity thresholding of Gaussian smoothed ($\sigma = 3$) versions of the GFP and GM130 maximum projection images. Threshold levels were determined independently for each data set. The soma mask was used to determine the neuron center of mass, and the neuron body and Golgi masks were used to ascertain which Golgi were included in the neuron of interest, requiring an 80% overlap of the mask regions. The neuron center of mass was used as a new coordinate origin, and a point was chosen on the base of the longest dendrite to define the zero-angle direction for subsequent processing. Using these axes, we mapped all GM130 images from Cartesian into polar coordinates, normalized by their total intensity and averaged. Golgi distribution images were created by converting back into Cartesian coordinates, with zero angle pointing up. Radial distributions were determined by taking the mean along the radial direction, leaving only intensity versus angle. The polarity index of somatic Golgi was calculated as the ratio of mean Golgi fluorescence intensity in quadrant 1 (Figures 3A and 3B) to the average of Golgi intensities in the remaining three quadrants.

Details about vesicle tracking and analysis of branchpoint Golgi are included in the Supplemental Data.

Statistical Analysis

Error bars represent the standard error of the mean. Statistical comparisons were two-sided t tests.

Supplemental Data

The Supplemental Data for this article can be found online at http://www.neuron.org/cgi/content/full/48/5/757/DC1/.

Acknowledgments

We dedicate this paper to the memory and inspiration of Larry Katz. We thank Ryan Irving, Irina Lebedeva, Kris Phend, and Haiwei Zhang for expert technical assistance. We thank Juliet Hernandez, Larry Katz, Fan Wang, and Jason Yi for helpful discussions and comments on the manuscript. M.D.E. is an Investigator of the Howard Hughes Medical Institute. In addition, this work was supported by grants to M.D.E. from the National Institutes of Health, the Christopher Reeve Paralysis Foundation, the Ruth K. Broad Foundation, and the Raymond and Beverly Sackler Foundation, as well as by the Gertrude Elion Award to A.C.H. from the Triangle Community Foundation. A.L.L. and E.E.M. are supported by DMR-0348910. B.R. and R.J.W. are supported by NS-35527.

Received: January 6, 2005
Revised: August 8, 2005
Accepted: November 4, 2005
Published: December 7, 2005

References

Aridor, M., Guzik, A.K., Bielli, A., and Fish, K.N. (2004). Endoplasmic reticulum export site formation and function in dendrites. J. Neurosci. *24*, 3770–3776.

Barr, F.A., Puype, M., Vandekerckhove, J., and Warren, G. (1997). GRASP65, a protein involved in the stacking of Golgi cisternae. Cell *91*, 253–262.

Bergmann, J.E., Kupfer, A., and Singer, S.J. (1983). Membrane insertion at the leading edge of motile fibroblasts. Proc. Natl. Acad. Sci. USA *80*, 1367–1371.

Brodie, C., Bogi, K., Acs, P., Lazarovici, P., Petrovics, G., Anderson, W.B., and Blumberg, P.M. (1999). Protein kinase C-epsilon plays a role in neurite outgrowth in response to epidermal growth factor and nerve growth factor in PC12 cells. Cell Growth Differ. *10*, 183–191.

Carnegie, G.K., Smith, F.D., McConnachie, G., Langeberg, L.K., and Scott, J.D. (2004). AKAP-Lbc nucleates a protein kinase D activation scaffold. Mol. Cell *15*, 889–899.

Dascher, C., and Balch, W.E. (1994). Dominant inhibitory mutants of ARF1 block endoplasmic reticulum to Golgi transport and trigger disassembly of the Golgi apparatus. J. Biol. Chem. *269*, 1437–1448.

de Anda, F.C., Pollarolo, G., Da Silva, J.S., Camoletto, P.G., Feiguin, F., and Dotti, C.G. (2005). Centrosome localization determines neuronal polarity. Nature *436*, 704–708.

Etienne-Manneville, S., and Hall, A. (2003). Cdc42 regulates GSK-3beta and adenomatous polyposis coli to control cell polarity. Nature *421*, 753–756.

Fache, M.P., Moussif, A., Fernandes, F., Giraud, P., Garrido, J.J., and Dargent, B. (2004). Endocytotic elimination and domain-selective tethering constitute a potential mechanism of protein segregation at the axonal initial segment. J. Cell Biol. *166*, 571–578.

Gardiol, A., Racca, C., and Triller, A. (1999). Dendritic and postsynaptic protein synthetic machinery. J. Neurosci. *19*, 168–179.

Goldberg, J.L., Klassen, M.P., Hua, Y., and Barres, B.A. (2002). Amacrine-signaled loss of intrinsic axon growth ability by retinal ganglion cells. Science *296*, 1860–1864.

Grueber, W.B., Jan, L.Y., and Jan, Y.N. (2003). Different levels of the homeodomain protein cut regulate distinct dendrite branching patterns of *Drosophila* multidendritic neurons. Cell *112*, 805–818.

Hand, R., Bortone, D., Mattar, P., Nguyen, L., Heng, J.I., Guerrier, S., Boutt, E., Peters, E., Barnes, A.P., Parras, C., et al. (2005). Phosphorylation of neurogenin2 specifies the migration properties and the dendritic morphology of pyramidal neurons in the neocortex. Neuron *48*, 45–62.

Hoogenraad, C.C., Milstein, A.D., Ethell, I.M., Henkemeyer, M., and Sheng, M. (2005). GRIP1 controls dendrite morphogenesis by regulating EphB receptor trafficking. Nat. Neurosci. *8*, 906–915.

Horch, H.W., and Katz, L.C. (2002). BDNF release from single cells elicits local dendritic growth in nearby neurons. Nat. Neurosci. *5*, 1177–1184.

Horton, A.C., and Ehlers, M.D. (2003). Dual modes of endoplasmic reticulum-to-Golgi transport in dendrites revealed by live-cell imaging. J. Neurosci. *23*, 6188–6199.

Horton, A.C., and Ehlers, M.D. (2004). Secretory trafficking in neuronal dendrites. Nat. Cell Biol. *6*, 585–591.

Hu, T., Kao, C.Y., Hudson, R.T., Chen, A., and Draper, R.K. (1999). Inhibition of secretion by 1,3-Cyclohexanebis(methylamine), a dibasic compound that interferes with coatomer function. Mol. Biol. Cell *10*, 921–933.

Jan, Y.N., and Jan, L.Y. (2003). The control of dendrite development. Neuron *40*, 229–242.

Jareb, M., and Banker, G. (1997). Inhibition of axonal growth by brefeldin A in hippocampal neurons in culture. J. Neurosci. *17*, 8955–8963.

Jontes, J.D., Buchanan, J., and Smith, S.J. (2000). Growth cone and dendrite dynamics in zebrafish embryos: early events in synaptogenesis imaged in vivo. Nat. Neurosci. *3*, 231–237.

Ju, W., Morishita, W., Tsui, J., Gaietta, G., Deerinck, T.J., Adams, S.R., Garner, C.C., Tsien, R.Y., Ellisman, M.H., and Malenka, R.C. (2004). Activity-dependent regulation of dendritic synthesis and trafficking of AMPA receptors. Nat. Neurosci. *8*, 244–253.

Kupfer, A., Dennert, G., and Singer, S.J. (1983). Polarization of the Golgi apparatus and the microtubule-organizing center within cloned natural killer cells bound to their targets. Proc. Natl. Acad. Sci. USA *80*, 7224–7228.

Lane, J.D., Lucocq, J., Pryde, J., Barr, F.A., Woodman, P.G., Allan, V.J., and Lowe, M. (2002). Caspase-mediated cleavage of the stacking protein GRASP65 is required for Golgi fragmentation during apoptosis. J. Cell Biol. *156*, 495–509.

Liljedahl, M., Maeda, Y., Colanzi, A., Ayala, I., Van Lint, J., and Malhotra, V. (2001). Protein kinase D regulates the fission of cell surface destined transport carriers from the trans-Golgi network. Cell *104*, 409–420.

Lin, C.Y., Madsen, M.L., Yarm, F.R., Jang, Y.J., Liu, X., and Erikson, R.L. (2000). Peripheral Golgi protein GRASP65 is a target of mitotic polo-like kinase (Plk) and Cdc2. Proc. Natl. Acad. Sci. USA *97*, 12589–12594.

Lippincott-Schwartz, J., Yuan, L.C., Bonifacino, J.S., and Klausner, R.D. (1989). Rapid redistribution of Golgi proteins into the ER in cells treated with brefeldin A: evidence for membrane cycling from Golgi to ER. Cell *56*, 801–813.

Maletic-Savatic, M., and Malinow, R. (1998). Calcium-evoked dendritic exocytosis in cultured hippocampal neurons. Part I: trans-Golgi network-derived organelles undergo regulated exocytosis. J. Neurosci. *18*, 6803–6813.

Mallard, F., Antony, C., Tenza, D., Salamero, J., Goud, B., and Johannes, L. (1998). Direct pathway from early/recycling endosomes to the Golgi apparatus revealed through the study of shiga toxin B-fragment transport. J. Cell Biol. *143*, 973–990.

Matlin, K.S., and Simons, K. (1983). Reduced temperature prevents transfer of a membrane glycoprotein to the cell surface but does not prevent terminal glycosylation. Cell *34*, 233–243.

McAllister, A.K., Katz, L.C., and Lo, D.C. (1997). Opposing roles for endogenous BDNF and NT-3 in regulating cortical dendritic growth. Neuron *18*, 767–778.

Murthy, M., Garza, D., Scheller, R.H., and Schwarz, T.L. (2003). Mutations in the exocyst component sec5 disrupt neuronal membrane traffic, but neurotransmitter release persists. Neuron *37*, 433–447.

Niell, C.M., Meyer, M.P., and Smith, S.J. (2004). In vivo imaging of synapse formation on a growing dendritic arbor. Nat. Neurosci. *7*, 254–260.

Nishimura, T., Kato, K., Yamaguchi, T., Fukata, Y., Ohno, S., and Kaibuchi, K. (2004). Role of the PAR-3-KIF3 complex in the establishment of neuronal polarity. Nat. Cell Biol. *6*, 328–334.

Pierce, J.P., Mayer, T., and McCarthy, J.B. (2001). Evidence for a satellite secretory pathway in neuronal dendritic spines. Curr. Biol. *11*, 351–355.

Polleux, F., Morrow, T., and Ghosh, A. (2000). Semaphorin 3A is a chemoattractant for cortical apical dendrites. Nature *404*, 567–573.

Prigozhina, N.L., and Waterman-Storer, C.M. (2004). Protein kinase D-mediated anterograde membrane trafficking is required for fibroblast motility. Curr. Biol. *14*, 88–98.

Sampo, B., Kaech, S., Kunz, S., and Banker, G. (2003). Two distinct mechanisms target membrane proteins to the axonal surface. Neuron *37*, 611–624.

Schwamborn, J.C., and Puschel, A.W. (2004). The sequential activity of the GTPases Rap1B and Cdc42 determines neuronal polarity. Nat. Neurosci. *7*, 923–929.

Shi, S.H., Jan, L.Y., and Jan, Y.N. (2003). Hippocampal neuronal polarity specified by spatially localized mPar3/mPar6 and PI 3-Kinase activity. Cell *112*, 63–75.

Shorter, J., and Warren, G. (1999). A role for the vesicle tethering protein, p115, in the post-mitotic stacking of reassembling Golgi cisternae in a cell-free system. J. Cell Biol. *146*, 57–70.

Spacek, J., and Harris, K.M. (1997). Three-dimensional organization of smooth endoplasmic reticulum in hippocampal CA1 dendrites and dendritic spines of the immature and mature rat. J. Neurosci. *17*, 190–203.

Sytnyk, V., Leshchyns'ka, I., Delling, M., Dityateva, G., Dityatev, A., and Schachner, M. (2002). Neural cell adhesion molecule promotes accumulation of TGN organelles at sites of neuron-to-neuron contacts. J. Cell Biol. *159*, 649–661.

Van Aelst, L., and Cline, H.T. (2004). Rho GTPases and activity-dependent dendrite development. Curr. Opin. Neurobiol. *14*, 297–304.

Waldron, R.T., and Rozengurt, E. (2003). Protein kinase C phosphorylates protein kinase D activation loop Ser744 and Ser748 and releases autoinhibition by the pleckstrin homology domain. J. Biol. Chem. *278*, 154–163.

Whitford, K.L., Dijkhuizen, P., Polleux, F., and Ghosh, A. (2002). Molecular control of cortical dendrite development. Annu. Rev. Neurosci. *25*, 127–149.

Wisco, D., Anderson, E.D., Chang, M.C., Norden, C., Boiko, T., Folsch, H., and Winckler, B. (2003). Uncovering multiple axonal targeting pathways in hippocampal neurons. J. Cell Biol. *162*, 1317–1328.

Yeaman, C., Ayala, M.I., Wright, J.R., Bard, F., Bossard, C., Ang, A., Maeda, Y., Seufferlein, T., Mellman, I., Nelson, W.J., and Malhotra, V. (2004). Protein kinase D regulates basolateral membrane protein exit from trans-Golgi network. Nat. Cell Biol. *6*, 106–112.

Yoshimura, S., Yoshioka, K., Barr, F.A., Lowe, M., Nakayama, K., Ohkuma, S., and Nakamura, N. (2005). Convergence of cell cycle regulation and growth factor signals on GRASP65. J. Biol. Chem. *280*, 23048–23056.